

Dynamic spin fluctuations at $T \rightarrow 0$ in a spin- $\frac{1}{2}$ ferromagnetic kagome lattice

Oren Ofer,^{1,*} Lital Marcipar,² V. Ravi Chandra,³ Snir Gazit,² Daniel Podolsky,² Daniel P. Arovav,⁴ and Amit Keren²

¹*Schulich Department of Chemistry, Technion - Israel Institute of Technology, Haifa 32000, Israel*

²*Department of Physics, Technion - Israel Institute of Technology, Haifa 32000, Israel*

³*School of Physical Sciences, National Institute of Science Education and Research, Institute of Physics Campus, Bhubaneswar 751005, India*

⁴*Department of Physics, University of California at San Diego, La Jolla, California 92093, USA*

(Received 3 December 2013; revised manuscript received 30 April 2014; published 16 May 2014)

We report magnetization, electron-spin resonance (ESR), and muon-spin relaxation (μ SR) measurements on single crystals of the $S = 1/2$ (Cu^{+2}) kagome compound $\text{Cu}(1,3\text{-benzodicarboxylate})$. The μ SR is carried to temperatures as low as 45 mK. The spin-Hamiltonian parameters are determined from the analysis of the magnetization and ESR data. We find that this compound has anisotropic ferromagnetic interactions. Nevertheless, no spin freezing is observed even at temperatures two orders of magnitude lower than the coupling constants. In light of this finding, the relation between persistent spin dynamics and spin liquids on kagome lattices is reexamined.

DOI: [10.1103/PhysRevB.89.205116](https://doi.org/10.1103/PhysRevB.89.205116)

PACS number(s): 75.10.Kt, 75.30.-m, 76.30.-v, 76.75.+i

The search for different kinds of quantum spin liquids (SLs) continues to draw considerable experimental attention, and new candidate SLs are reported from time to time [1–9]. Much of the search is focused on compounds with a kagome lattice. SLs lack long-range order and are classified according to the presence or absence of a gap to magnetic excitations. The gapless ones, or those with a gap smaller than the lowest experimentally available temperature, are expected to have persistent spin dynamics (PSD) at $T \rightarrow 0$. A major experimental tool in the search for such states is the muon-spin relaxation (μ SR) technique. μ SR is ideal for this task since it operates at zero external field, without affecting the rotation symmetry of the Hamiltonian. In addition, μ SR can detect the presence of long-range order and dynamic fluctuations. PSD in μ SR is manifested as a temperature-independent spin fluctuation below some characteristic temperature. It has been frequently used to identify materials such as SLs. However, μ SR detected PSD in some compounds that are not necessarily SLs, such as pyrochlores [10] and molecular magnets [11]. This observation raises a question: Can μ SR give a false-positive observation when used to identify a SL?

To address this question, we investigate the organometallic hybrid kagome compound $\text{Cu}(1,3\text{-benzodicarboxylate})$ [$\text{Cu}(1,3\text{-bdc})$]. This compound, with the chemical formula $\text{Cu}_8\text{H}_4\text{O}_4$, has the ideal qualities of a spin-1/2 kagome featuring a nonmagnetic 1,3-bdc ligand which links the Cu^{+2} kagome layers [12]. Initial magnetization measurements on polycrystalline samples of $\text{Cu}(1,3\text{-bdc})$ suggested that the mean nearest-neighbor superexchange interaction is antiferromagnetic (AFM) in nature with a Curie-Weiss (CW) temperature of $\Theta_{\text{CW}} = -33$ K, yet at low temperatures the onset of a ferromagnetic (FM) signal was observed [12]. Recently, neutron-scattering data were presented, confirming this magnetic state [13]. Ferromagnetic correlation on a kagome lattice means that the degree of frustration is low, and therefore the spins should freeze at low temperatures. Nevertheless, early μ SR measurements showed only slowing down of the spin fluctuations below $T_s = 1.8$ K. The measurements were

carried out down to 0.9 K, where the magnetic state remains dynamic with no signs of long-range order [14].

Here we study single crystals synthesized in the form of millimeter-size flakes [12]. We combine direction-dependent bulk magnetization and electron-spin resonance (ESR) measurements to characterize the spin Hamiltonian of these crystals. We show that $\text{Cu}(1,3\text{-bdc})$ is an anisotropic, slightly frustrated ferromagnet; it is certainly not a SL. We also extend the temperature dependence of the previous μ SR measurements and show that the dynamic fluctuations persist down to 45 mK. This result indicates that PSD detected by μ SR can give a false positive when used to identify a SL state.

The bulk magnetization (M) measurements were performed using a commercial superconducting quantum interference device (SQUID) at temperatures $3 \leq T \leq 140$ K with external fields between $0.1 \leq H \leq 25$ kG applied along and perpendicular to the kagome planes, i.e., $\mathbf{H} \parallel \hat{\mathbf{c}}$ and $\mathbf{H} \perp \hat{\mathbf{c}}$. The crystals were held onto a small flat glass using epoxy glue with the $\hat{\mathbf{c}}$ direction perpendicular to the glass. The $\hat{\mathbf{c}}$ direction is also perpendicular to the kagome plane. The crystal's $\hat{\mathbf{a}}$ and $\hat{\mathbf{b}}$ directions are random. To determine the background signal, we measured the contribution from an identical glass with the epoxy (not shown). This measurement indicated no temperature dependence and a negligible background contribution compared to the sample signal.

The magnetization measurements versus field at a temperature of $T = 2.4$ K, for two field directions, are plotted in Fig. 1. At fields higher than about 15 kG, the magnetization saturates for both directions. For $\mathbf{H} \perp \hat{\mathbf{c}}$, the saturation is reached at a lower field than for $\mathbf{H} \parallel \hat{\mathbf{c}}$. This means that the generated internal fields are strongest when the spins are in the kagome plane. The saturation value of the magnetization is $1.231(5)\mu_B$. This suggests that the g factor is higher than 2. For a free spin 1/2, the field dependence of the magnetization $\mathbf{M} = g\mu_B \langle \mathbf{S} \rangle$ is given by the Brillouin function. This function is plotted in Fig. 1 by the dash-dotted line. Clearly the magnetization saturates at lower applied fields than expected for noninteracting spins in both directions. This means that the internal field is larger than the external one and that $\text{Cu}(1,3\text{-bdc})$ is a ferromagnet in our experimental conditions.

*oren@physics.technion.ac.il

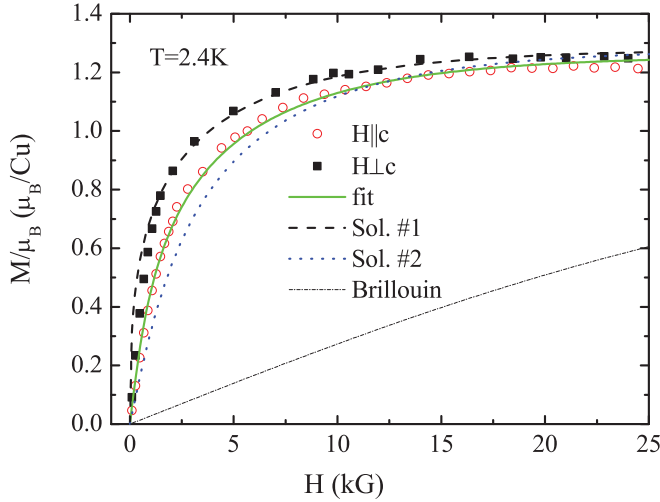


FIG. 1. (Color online) Magnetization of Cu(1,3-bdc) at $T = 2.4$ K, measured at two directions of the crystal: $\mathbf{H} \parallel \hat{\mathbf{c}}$ (black filled symbols) and $\mathbf{H} \perp \hat{\mathbf{c}}$ (red hollow symbols). The dash-dotted line indicates a spin-1/2 Brillouin function with $g = 2.0023$. The solid line indicates a fit to a Brillouin function with an effective field [see Eq. (2)]. The dashed (dotted) curves show the Brillouin function with an effective field using two possible derived Hamiltonian parameters given in Table I.

To take interactions into account, we consider a fully anisotropic nearest-neighbor exchange Hamiltonian,

$$\mathcal{H} = \sum_{\langle i,j \rangle} [J\mathbf{S}_i \cdot \mathbf{S}_j + DS_i^z S_j^z + E(S_i^x S_j^x - S_i^y S_j^y) + F(\mathbf{S}_i \times \mathbf{S}_j)_z] - g\mu_B \sum_i \mathbf{S}_i \cdot \mathbf{H}, \quad (1)$$

where the sum is over nearest-neighbor bonds, J is the exchange coupling, E and D are the anisotropies, and F represents the $\hat{\mathbf{z}}$ component of the Dzyaloshinskii-Moriya (DM) term [15], which is often the biggest [16]. The $\hat{\mathbf{x}}$ direction is along each bond, the $\hat{\mathbf{y}}$ direction is in the kagome plane perpendicular to each bond, and the $\hat{\mathbf{z}}$ direction is perpendicular to the kagome plane. D , E , and F are believed to be due to spin-orbit couplings. F is a first-order and E and D are second-order effects. Nevertheless, E and D generate differences in the high-temperature magnetization between different directions, which, as we show below, occur in our system. Therefore, E and D are certainly part of the Hamiltonian [17]. We start our analysis by assuming $F = 0$, and, as we shall see, there will be no reason to relax this assumption.

In the mean-field approximation, the magnetization on each of the three kagome sublattices d is determined by the effective field that this sublattice experiences, $\mathbf{H}_{\text{eff}}^d$. This field is due to the external field and the internal field generated by the moments \mathbf{M}^d of the other sublattices, and is given by the generalized Brillouin function

$$\mathbf{M}^d = \frac{g_{\hat{\mathbf{H}}} \mu_B}{2} \tanh\left(\frac{g_{\hat{\mathbf{H}}} \mu_B}{2k_B T} |\mathbf{H}_{\text{eff}}^d|\right) \hat{\mathbf{H}}_{\text{eff}}^d, \quad (2)$$

where $g_{\hat{\mathbf{H}}}$ represents the direction-dependent g factor. When the external field is in the $\hat{\mathbf{z}}$ direction, all sublattices are

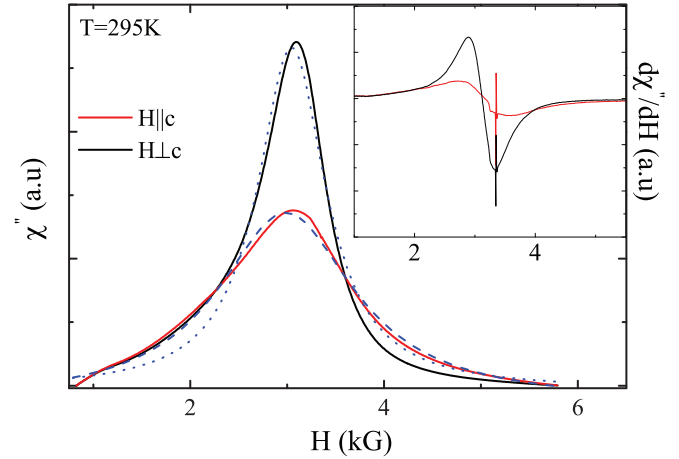


FIG. 2. (Color online) Representative ESR data for the two measured directions, $\mathbf{H} \parallel \hat{\mathbf{c}}$ (red) and $\mathbf{H} \perp \hat{\mathbf{c}}$ (black), taken at $T = 295$ K. The inset displays the ESR raw signal. The main panel shows the integrated signal (absorption line). The dashed lines demonstrate the fit to a Lorentzian function.

magnetized in that direction only, their moments are equal, and

$$\mathbf{H}_{\text{eff}} = [H - z(J + D)M_z / (g\mu_B)^2] \hat{\mathbf{z}}, \quad (3)$$

regardless of d ; z is the number of neighbors. A solution of the implicit Eqs. (2) and (3) generates $M_z(H, J, D, g_{\parallel})$. We fit this M_z to the $\mathbf{H} \parallel \hat{\mathbf{c}}$ data and find that

$$J + D = -2.04(2) \text{ K}, \quad (4)$$

and $g_{\parallel} = 2.51(1)$. The fit is plotted in Fig. 1 by the solid line. The calculated magnetization with interactions describes the data quite well. This calculation demonstrates that the interactions in the $\hat{\mathbf{z}}$ direction must be ferromagnetic on the order of 1 K.

Other Hamiltonian parameters are obtained from ESR. The ESR measurements were done in the X band ($\omega_0 = 9.5$ GHz) at $15 \leq T \leq 300$ K. The applied field was swept between $0.9 \leq H \leq 6$ kG. The inset in Fig. 2 plots representative raw ESR data taken at $T = 295$ K of the sample with a diphenylpicrylhydrazyl (DPPH) reference. To obtain the absorption line, we subtract the reference signal and integrate the raw ESR signal over the applied field. The main panel of Fig. 2 shows the absorption lines for the two measured directions. A reasonable fit to the absorption line is found to be a Lorentzian function,

$$\chi''(H) = \frac{A_{\parallel,\perp}}{\pi} \frac{\delta}{\delta^2 + (H - H_{\parallel,\perp})^2}, \quad (5)$$

where 2δ is the full width at half maximum and $H_{\parallel,\perp} = \omega_0 / (g_{\parallel,\perp} \mu_B)$ is the resonance field. We find that $g_{\perp} = 2.164(2)$, $g_{\parallel} = 2.181(2)$, $\delta_{\perp} = 0.432(1)$ kG, and $\delta_{\parallel} = 0.867(22)$ kG. The δ and g factor do not have temperature dependence down to 15 K. The area A of the $\mathbf{H} \perp \hat{\mathbf{c}}$ measurement is highest, consistent with the magnetization data, and increases upon cooling as expected. The ESR $g_{\parallel,\perp}$ factors are larger than 2, but lower than the value determined by the magnetization measurement. The cause of the discrepancy

TABLE I. The Hamiltonian parameters derived from the solution of Eqs. (6) and (4).

Solution No.	J (K)	D (K)	E (K)
1	-2.3822	0.3421	± 0.14217
2	-1.7470	-0.2930	± 0.12175

between the magnetization and ESR g factors is not clear to us.

At temperature higher than typical interaction strength, the widths δ_{\parallel} and δ_{\perp} are related to the three Hamiltonian parameters via the moments according to

$$g_{\parallel,\perp} \mu_B \delta_{\parallel,\perp} = \frac{\pi}{\sqrt{3}} M_2^{\parallel,\perp} \sqrt{\frac{M_2^{\parallel,\perp}}{M_4^{\parallel,\perp}}}, \quad (6)$$

where $M_2^{\parallel,\perp} = -\text{Tr}([\mathcal{H}, S_{\perp,\parallel}]^2)/\text{Tr}(S_{\perp,\parallel}^2)$ and $M_4^{\parallel,\perp} = \text{Tr}([\mathcal{H}, [\mathcal{H}, S_{\perp,\parallel}]]^2)/\text{Tr}(S_{\perp,\parallel}^2)$ are the second and fourth moments, respectively, and $S_{\perp,\parallel}$ stands for the spin component perpendicular or parallel to the applied field, respectively. For the Hamiltonian of Eq. (1), on a kagome lattice, and for each of the field orientations, we obtain the second and fourth moments as given in Sec. 1 of the Appendix. When taking $F = 0$, the second moments are given by

$$M_2^{\perp} = 4E^2, \quad (7)$$

$$M_2^{\parallel} = E^2 + D^2, \quad (8)$$

and the fourth moments up to second order in anisotropies are given by

$$M_4^{\perp} = 18J^2E^2, \quad (9)$$

$$M_4^{\parallel} = \frac{9}{2}J^2E^2 + 3J^2D^2. \quad (10)$$

We numerically solve Eqs. (6) and (4). All of the possible solutions of these equations are given in Table I.

In both solutions, $J + D < 0$ and $J \pm E < 0$ and, as stated above, the interactions between spins are ferromagnetic in all directions.

To check our conclusion and to verify the assumption made so far, we use the calculated Hamiltonian parameters to generate the expected field-dependent magnetization in the perpendicular direction, $\langle M_{\perp} \rangle (H, J, E, g_{\perp})$, and compare it to the data in Fig. 1. For this purpose, we calculate the two-component magnetization of each of the three kagome sublattices \mathbf{M}^d for $\mathbf{H} \perp \hat{\mathbf{c}}$ by solving the six coupled explicit Eqs. (2). The $\mathbf{H}_{\text{eff}}^d$ expressions are given in Sec. 2 of the Appendix. We then average the magnetization on the three sublattices and project the result onto the $\hat{\mathbf{H}}$ direction to generate $\langle M_{\perp} \rangle$ as measured experimentally. For all applied field values, the result is independent of the applied field direction in the plane. The g factor determined from the high field data is $g_{\perp} = 2.55(4)$. In Fig. 1, we show the calculated $\langle M_{\perp} \rangle$ for the two possible sets of parameters from Table I. Only solution 1 in the table agrees with the data. The agreement with

the data is nearly perfect. Therefore, one can fit all our data without the need to introduce F .

We attempt to confirm these results by temperature-dependent susceptibility $\chi \equiv M/H$ measurements for $H \rightarrow 0$. However, the susceptibility measurements are not conclusive. They are presented and discussed in Sec. 3 of the Appendix.

We now turn to discuss the longitudinal fields (LFs) μSR results. The data were collected at the M15 surface muon beam line at TRIUMF using a dilution refrigerator spectrometer. The spectra were gathered at $T = 45$ and $T = 240$ mK. In the LF mode, the external field is applied along the initial muon-spin direction. When the internal fields fluctuate in space and time, the muon-spin polarization is expected to complete less than one full oscillation, and then relax. The frequency of oscillation increases and the relaxation rate decreases as the field increases. This behavior is described by the dynamical LF Kubo-Toyabe (DLFKT) function $G(\Delta, \nu, t, H_{\text{LF}})$, where ν is the field fluctuation rate, Δ is the static width of the local field distribution, and H_{LF} is the applied field [18].

Figure 3(a) shows the spectra obtained with different fields at $T = 45$ mK. The data exhibits a typical DLFKT behavior in every respect. We fit the function

$$A(t) = A_0 G(\Delta, \nu, t, H_{\text{LF}}) + B_g \quad (11)$$

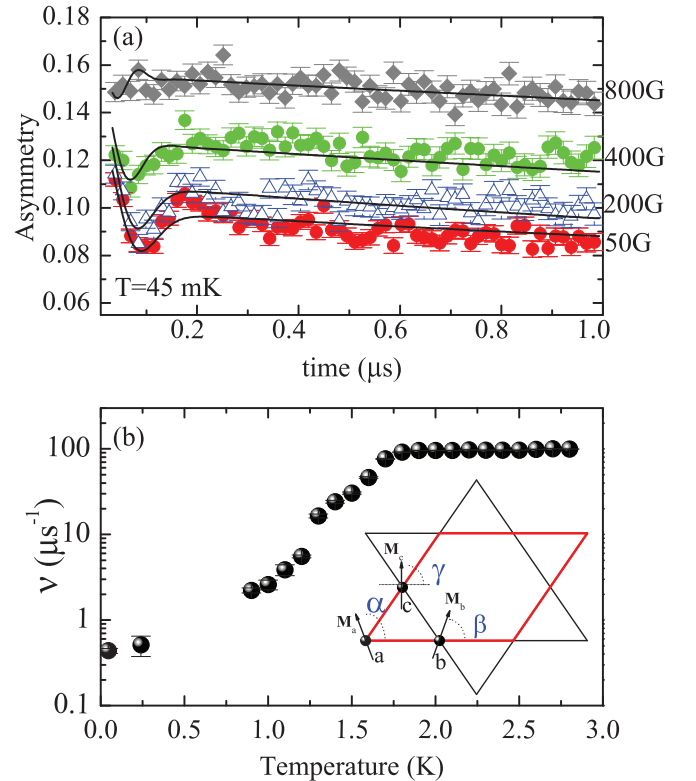


FIG. 3. (Color online) (a) The raw μSR data with applied longitudinal field of 50 to 800 G; the solid lines demonstrate the fit to Eq. (11). (b) A semilogarithmic scale of the spins fluctuation rate ν obtained in Ref. [14] with the added points at 240 and 45 mK. Inset: The kagome unit cell (bold red) with its three sublattices (a, b, and c), the corresponding magnetic moment (\mathbf{M}^a , \mathbf{M}^b , and \mathbf{M}^c), and angles (α , β , γ).

to the data, where A_0 is the asymmetry from muons in the sample and B_g is a nonrelaxing background due to muons stopping in the sample holder. All of the fit parameters are shared for all of the data sets at a given temperature. The instantaneous internal field distribution is assumed to be Gaussian. The fit is demonstrated by the solid lines in Fig. 3(a). We obtain that $\nu = 0.43(2)\mu\text{s}^{-1}$ and $\Delta = 19.3450(4)$ MHz. The value for Δ is consistent with previous measurements [14], indicating the same field distribution from the millidegrees Kelvin to few Kelvin range. In contrast, ν decreases by a factor of ≈ 8 relative to data obtained before at a temperature 20 times larger (0.9 K) [14]. We add the new ν values to the previous results in Fig. 3(b). The full picture clearly shows dramatic slowing of the spin fluctuations below ≈ 1.8 K. However, the system continues to fluctuate even at 0.05 K with no signs of freezing. Between 240 and 45 mK, ν is finite, clearly measurable by μSR , and temperature independent.

It should be pointed out that the analysis of the μSR data was done assuming that the muon experiences only the external field. In a ferromagnet, the local field in the muon site is larger than the external one. Without proper knowledge of the muon stopping site, it is difficult to estimate this local field. Nevertheless, the successful fit with H_L as the local field suggests that the internal contribution to the local field is much smaller than H_L . In any case, analysis of our data with a field larger than H_{LF} could only lead to higher values of ν . Therefore, the ν in Fig. 3(b) should be considered as the lower limit on the real values.

The absence of frozen moment and finite fluctuation rate ν at $T \rightarrow 0$, on different time scales, was observed in many kagome lattices with antiferromagnetic interactions such as SCGO [1], Volborthite [2,3], Herbertsmithite [4,5], $\text{Nd}_3\text{Ga}_5\text{SiO}_{14}$ [6], Langasite [7], Kapellasite [8], and vanadium-oxyfluoride [9]. All of these compounds are considered to be a SL. However, the Hamiltonian in Eq. (1), with the parameters in Table I, gives a ground state that is fundamentally different from these spin liquids. Since $D > |E|$, the spins lie in the xy plane. This allows us to define one angle per spin, as shown in the inset of Fig. 3(b). For positive or negative E , the spins would prefer to lie parallel or perpendicular to a bond, respectively. However, the ground-state energy minimum is reached when two spins make the angles $\alpha = -\beta = -\sqrt{3}E/(6J - E)$ with a bond, and the third spin has $\gamma = 0$ and is 60 degrees away from a bond (see Sec. 4 of the Appendix). This is a slightly frustrated spin arrangement. A new energy minimum for all the spins on the lattice is found every 60 degrees, but there is no local continuous degeneracy. The energy minimum is shallow and it takes ~ 10 mK per unit cell to overcome the potential barrier and move the entire spin system collectively between local energy minima. This means that Cu(1,3-bdc) should order magnetically and it is not a spin liquid, yet it produces the same μSR signature as a SL.

In summary, the Cu(1,3-bdc), with Cu^{+2} spin-1/2 situated on a kagome lattice, exhibits anisotropic but ferromagnetic interactions in all directions. μSR does not detect long-range order and indicates persistent spin dynamics down to 45 mK, as expected from a spin liquid. The same behavior was observed in many kagome lattices with AFM interactions. The absence of muon-spin oscillations can be assigned to

multiple muon sites. However, the PSD is very surprising since a kagome lattice with ferromagnetic interactions has a very small degree of frustration, lacks continuous local degeneracy, and is not a spin liquid. Thus, our experiment suggests that μSR on its own can falsely identify spin liquid on a kagome lattice. Cu(1,3-bdc) is an example of a kagome system with long-range magnetic order and PSD at $T \rightarrow 0$. This unusual behavior could be a new effect or a result of excitations caused by the muon itself as it is introduced into the sample.

This work was supported by the Israel USA Binational Science Foundation. We would like to thank Young S. Lee and Joel S. Helton for providing us with the samples. The authors wish to thank the TRIUMF staff for help with the μSR experiments. Helpful discussions with Sarah Dunsiger are greatly acknowledged.

APPENDIX

In this Appendix, we expand some of the results used in the main text.

1. Moments

The evaluation of the linewidths in ESR at high temperatures involves calculating the second- and fourth-order moments to be used in Eq. (6) in the main text. Thus we need to evaluate the first- and second-order commutators of the total spin component in a given direction and the Hamiltonian. It is straightforward to see that for a spin-1/2 Hamiltonian, the first-order commutator gives rise to two-spin terms. The second-order commutator gives rise to single-spin or three-spin terms, depending on whether a bond term, from the Hamiltonian, and a two-spin term, from the first-order commutator, share two sites or one.

The evaluation of the traces involves careful bookkeeping of all the different terms possible. We accomplished that by writing a *Mathematica* program which evaluates all the terms that can arise and computes the trace. The program evaluates the moments for a general Hamiltonian of spin-1/2 sites. It is assumed that the lattice can be grouped into clusters of sites, which can be seen as sublattices corresponding to a particular Bravais lattice site. The Hamiltonian is then specified as the sum of interactions within a cluster and between clusters. Thus we assume that the Hamiltonian has translation invariance. The input to the program specifies all the site indices and coupling coefficients (nine in number, for $S_{i\alpha}S_{j\beta}$) for all the different bonds involving spins from the Bravais lattice site at the origin. The rest of the bonds on the lattice and their contributions to the trace can be evaluated given the translation invariance. Thus the evaluation is quite general and can be extended to several other systems with more general Hamiltonians, such as those containing all the components of the DM interaction and also longer-range exchange interactions.

The moments in this paper have been evaluated for the anisotropic kagome Hamiltonian with three exchange-coupling constants and a Dzyaloshinski-Moriya (DM) term

given in Eq. (1) of the main text. They are given by

$$M_2^\perp = 4E^2, \quad (\text{A1})$$

$$M_2^\parallel = F^2 + E^2 + D^2, \quad (\text{A2})$$

$$M_4^\perp = 18J^2E^2 + 28E^4 + 10F^2E^2 + 8\sqrt{3}FE^2J \\ + 4\sqrt{3}FE^2D + 20JDE^2 + 8E^2D^2, \quad (\text{A3})$$

$$M_4^\parallel = \frac{11}{2}F^4 - JDE^2 + \frac{9}{2}J^2E^2 + 3J^2D^2 \\ + 2JD^3 - \frac{5\sqrt{3}}{2}FE^2D + \frac{13}{4}E^4 + \frac{5}{2}D^4 \\ + \frac{41}{4}F^2E^2 + 2F^2J^2 + 3F^2D^2 + \frac{25}{4}E^2D^2. \quad (\text{A4})$$

2. Effective fields

The kagome lattice is constructed from three sublattices. They are presented in Fig. 3(b) of the paper. The effective fields in the three different sublattices are

$$\mathbf{H}_{\text{eff}}^a = \mathbf{H} - \frac{2J}{g^2\mu_B^2}(\mathbf{M}^b + \mathbf{M}^c) - \frac{E}{g^2\mu_B^2}(2M_x^b \\ - M_x^c + \sqrt{3}M_y^c, -2M_y^b + M_y^c + \sqrt{3}M_x^c), \quad (\text{A5})$$

$$\mathbf{H}_{\text{eff}}^b = \mathbf{H} - \frac{2J}{g^2\mu_B^2}(\mathbf{M}^a + \mathbf{M}^c) - \frac{E}{g^2\mu_B^2}(2M_x^a \\ - M_x^c - \sqrt{3}M_y^c, -2M_y^a + M_y^c - \sqrt{3}M_x^c), \quad (\text{A6})$$

$$\mathbf{H}_{\text{eff}}^c = \mathbf{H} - \frac{2J}{g^2\mu_B^2}(\mathbf{M}^b + \mathbf{M}^a) - \frac{E}{g^2\mu_B^2}(-M_x^a \\ - M_x^b + \sqrt{3}M_y^a - \sqrt{3}M_y^b, M_y^a + M_y^b \\ + \sqrt{3}M_x^a - \sqrt{3}M_x^b). \quad (\text{A7})$$

3. Susceptibility

The inverse susceptibility χ^{-1} as a function of temperature, for both field orientations with an applied field of 0.1 kG, is depicted in Fig. 4. χ^{-1} is clearly different between the two directions. We performed a high-temperature fit to the inverse Curie-Weiss (CW) law, $\chi(T)^{-1} = (T - \Theta_{\text{CW}})/C$, where C is the Curie constant and Θ_{CW} is the CW temperature. For the two experiments, the fit was applied in two temperature ranges: low T [5 K, 30 K] and high T [50 K, 100 K]. Above 100 K, $\chi(T)^{-1}$ is no longer linear with T for both directions. The CW temperature for $\mathbf{H} \parallel \hat{c}$ from the high- T range is $-1.0(8)$ K, and from the low- T range, it is $\Theta_{\text{CW}}^\parallel = 4.03$ K. The CW temperature for $\mathbf{H} \perp \hat{c}$ from the high T is $\Theta_{\text{CW}}^\perp = -49(2)$ K. For low T , $\mathbf{H} \perp \hat{c}$, the data is not linear and could not be fitted reliably. The inset of Fig. 4 displays the difference between the fitted curve and the experimental data. This difference for $[\chi(T)^\perp]^{-1}$ deviates greatly from 0, whereas the difference for $[\chi(T)^\parallel]^{-1}$ is close to 0. This type of analysis provides a reliable Θ_{CW} only when the temperature range used in the fit is much

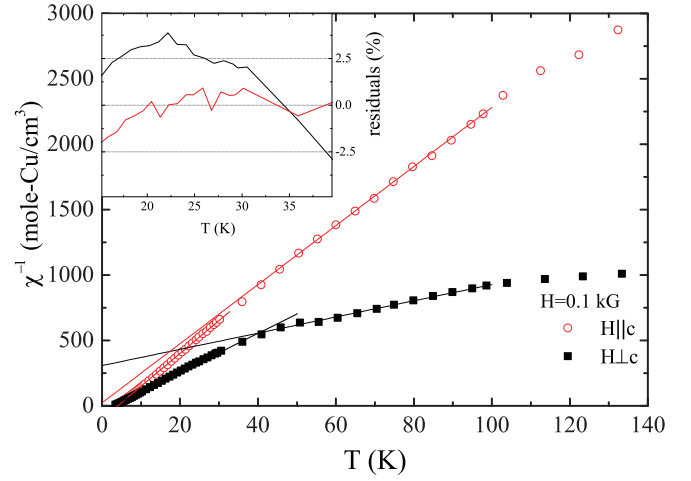


FIG. 4. (Color online) The temperature dependence of the inverse susceptibility $\chi^{-1}(T)$, measured at two directions: $\mathbf{H} \parallel \hat{c}$ (filled symbols) and $\mathbf{H} \perp \hat{c}$ (hollow symbols); the solid lines are fits to a the inverse Curie-Weiss law. The inset shows the residuals from the fit at low temperatures.

larger than the CW temperature obtained by the fit. For $\mathbf{H} \perp \hat{c}$, this condition is not obeyed in the high-temperature range. Therefore, Θ_{CW}^\perp is ambiguous. For $\mathbf{H} \parallel \hat{c}$, both temperature ranges are valid, but give conflicting values of $\Theta_{\text{CW}}^\parallel$.

The situation is even more confusing when analyzing the Curie constant for the different directions and temperature ranges. We found that in both temperature ranges, the Curie constant is substantially different between the different directions, and much smaller than expected from localized spin 1/2 on each Cu site. We therefore abandon susceptibility measurements as a means of characterizing the Hamiltonian.

4. Ground state

We determine the ground state in the mean-field approximation by writing

$$\mathbf{M}_a = M(\cos \alpha, \sin \alpha), \quad (\text{A8})$$

$$\mathbf{M}_b = M(\cos \beta, \sin \beta), \quad (\text{A9})$$

$$\mathbf{M}_c = M(\cos \gamma, \sin \gamma). \quad (\text{A10})$$

The Hamiltonian per unit cell $H = -\frac{1}{2}(\mathbf{M}_a \cdot \mathbf{H}_a^{\text{eff}} + \mathbf{M}_b \cdot \mathbf{H}_b^{\text{eff}} + \mathbf{M}_c \cdot \mathbf{H}_c^{\text{eff}})$ in zero external field is given by

$$H = \frac{M^2}{2(g\mu_B)^2} \{ J[4 \cos(\alpha - \beta) + 4 \cos(\beta - \gamma) \\ + 4 \cos(\gamma - \alpha)] + E[4 \cos(\alpha + \beta) + 2\sqrt{3} \sin(\alpha + \gamma) \\ - 2\sqrt{3} \sin(\beta + \gamma) - 2 \cos(\alpha + \gamma) - 2 \cos(\beta + \gamma)] \}. \quad (\text{A11})$$

This Hamiltonian is invariant under rotations by 120 degrees and cyclic permutations of the angles. Numerical search for the minimum shows that it occurs at $\alpha = -\beta$ and $\gamma = 0$. Given these relations, and that for each sublattice $\mathbf{H}_d^{\text{eff}}$ is parallel to \mathbf{M}_d , we find that $\alpha = -\beta = -\sqrt{3}E/(6J - E)$.

- [1] Y. J. Uemura, A. Keren, K. Kojima, L. P. Le, G. M. Luke, W. D. Wu, Y. Ajiro, T. Asano, Y. Kuriyama, M. Mekata, H. Kikuchi, and K. Kakurai, *Phys. Rev. Lett.* **73**, 3306 (1994).
- [2] A. Fukaya, Y. Fudamoto, I. M. Gat, T. Ito, M. I. Larkin, A. T. Savici, Y. J. Uemura, P. P. Kyriakou, G. M. Luke, M. T. Rovers, K. M. Kojima, A. Keren, M. Hanawa, and Z. Hiroi, *Phys. Rev. Lett.* **91**, 207603 (2003).
- [3] F. Bert, D. Bono, P. Mendels, J.-C. Trombe, P. Millet, A. Amato, C. Baines, and A. Hillier, *J. Phys.: Condens. Matter* **16**, S829 (2004).
- [4] P. Mendels, F. Bert, M. A. de Vries, A. Olariu, A. Harrison, F. Duc, J. C. Trombe, J. S. Lord, A. Amato, and C. Baines, *Phys. Rev. Lett.* **98**, 077204 (2007).
- [5] Oren Ofer, Amit Keren, E. A. Nytko, M. P. Shores, B. M. Bartlett, D. G. Nocera, C. Baines, and A. Amato, [arXiv:cond-mat/0610540v2](https://arxiv.org/abs/cond-mat/0610540v2).
- [6] A. Zorko, F. Bert, P. Mendels, P. Bordet, P. Lejay, and J. Robert, *Phys. Rev. Lett.* **100**, 147201 (2008).
- [7] A. Zorko, F. Bert, P. Mendels, K. Marty, and P. Bordet, *Phys. Rev. Lett.* **104**, 057202 (2010).
- [8] B. Fåk, E. Kermarrec, L. Messio, B. Bernu, C. Lhuillier, F. Bert, P. Mendels, B. Koteswararao, F. Bouquet, J. Ollivier, A. D. Hillier, A. Amato, R. H. Colman, and A. S. Wills, *Phys. Rev. Lett.* **109**, 037208 (2012).
- [9] L. Clark, J. C. Orain, F. Bert, M. A. De Vries, F. H. Aidoudi, R. E. Morris, P. Lightfoot, J. S. Lord, M. T. F. Telling, P. Bonville, J. P. Attfield, P. Mendels, and A. Harrison, *Phys. Rev. Lett.* **110**, 207208 (2013).
- [10] P. Dalmas de Reotier, A. Yaouanc, L. Keller, A. Cervellino, B. Roessli, C. Baines, A. Forget, C. Vaju, P. C. M. Gubbens, A. Amato, and P. J. C. King, *Phys. Rev. Lett.* **96**, 127202 (2006); A. Yaouanc, P. Dalmas de Réotier, P. Bonville, J. A. Hodges, V. Glazkov, L. Keller, V. Sikolenko, M. Bartkowiak, A. Amato, C. Baines, P. J. C. King, P. C. M. Gubbens, and A. Forget, *ibid.* **110**, 127207 (2013); J. S. Gardner, S. R. Dunsiger, B. D. Gaulin, M. J. P. Gingras, J. E. Greedan, R. F. Kiefl, M. D. Lumsden, W. A. MacFarlane, N. P. Raju, J. E. Sonier, I. Swainson, and Z. Tun, *ibid.* **82**, 1012 (1999); A. Keren, J. S. Gardner, G. Ehlers, A. Fukaya, E. Segal, and Y. J. Uemura, *ibid.* **92**, 107204 (2004).
- [11] A. Lascialfari, Z. H. Jang, F. Borsa, P. Carretta, and D. Gatteschi, *Phys. Rev. Lett.* **81**, 3773 (1998); Zaher Salman, Amit Keren, Philippe Mendels, Valerie Marvaud, Ariane Sculler, Michel Verdagner, James S. Lord, and Chris Baines, *Phys. Rev. B* **65**, 132403 (2002).
- [12] Emily A. Nytko, Joel S. Helton, Peter Muller, and D. G. Nocera, *J. Am. Chem. Soc.* **130**, 2922 (2008).
- [13] Robin Chisnell (private communication).
- [14] L. Marcipar, O. Ofer, A. Keren, E. A. Nytko, D. G. Nocera, Y. S. Lee, J. S. Helton, and C. Bains, *Phys. Rev. B* **80**, 132402 (2009).
- [15] M. Elhajal, B. Canals, and C. Lacroix, *Phys. Rev. B* **66**, 014422 (2002).
- [16] A. Zorko, S. Nellutla, J. van Tol, L. C. Brunel, F. Bert, F. Duc, J.-C. Trombe, M. A. de Vries, A. Harrison, and P. Mendels, *Phys. Rev. Lett.* **101**, 026405 (2008).
- [17] Oren Ofer and Amit Keren, *Phys. Rev. B* **79**, 134424 (2009).
- [18] R. S. Hayano, Y. J. Uemura, J. Imazato, N. Nishida, T. Yamazaki, and R. Kubo, *Phys. Rev. B* **20**, 850 (1979).